Composites Part B 217 (2021) 108901

Contents lists available at ScienceDirect

Composites Part B

journal homepage: www.elsevier.com/locate/compositesb

Hydrogen-bonded network enables polyelectrolyte complex hydrogels with high stretchability, excellent fatigue resistance and self-healability for human motion detection

Hui Song [a], Yinglun Sun [c], Jixin Zhu [d], Jingsan Xu [e], Chao Zhang [a,*], Tianxi Liu [a,b,**]

[a] State Key Laboratory for Modification of Chemical Fibers and Polymer Materials, College of Materials Science and Engineering, Donghua University, Shanghai, 201620, China
[b] Key Laboratory of Synthetic and Biological Colloids, Ministry of Education, School of Chemical and Material Engineering, Jiangnan University, Wuxi, 214122, China
[c] Laboratory of Clean Energy Chemistry and Materials, Lanzhou Institute of Chemical Physics, Chinese Academy of Sciences, Lanzhou, 730000, China
[d] Shaanxi Institute of Flexible Electronics (SIFE), Northwestern Polytechnical University (NPU), 127 West Youyi Road, Xi'an, 710072, China
[e] School of Chemistry, Physics and Mechanical Engineering, Queensland University of Technology, Brisbane, QLD, 4001, Australia

ARTICLE INFO

Keywords:
Ion conductive hydrogels
Hydrogen-bonded network
Polyelectrolyte complex hydrogel
Stretchability
Fatigue resistance
Wearable strain sensor

ABSTRACT

Polyelectrolyte complex hydrogel (PECH) is an emerging ion conductive hydrogel made from non-covalent interacted oppositely charged polyelectrolytes in water. However, the construction of PECH with high stretchability, excellent fatigue resistance and self-healability is heavily demanded while remaining a profound challenge. Herein, a hydrogen-bonded network densification strategy is presented for preparing a highly stretchable and deformation-tolerant PECH hydrogel (Fe/CS/PAA), which is composed of an anionic Fe^{3+}-coordinated polyacrylic acid network (Fe-PAA) and cationic Fe^{3+}-coordinated chitosan network (Fe-CS). Benefiting from the formation of dense hydrogen-bonded network between the Fe-PAA and Fe-CS networks activated by salt impregnation, the resultant densified hydrogen-bonded Fe/CS/PAA hydrogel (DHB-Fe/CS/PAA) exhibits large tensile strength (~0.34 MPa), high stretchability (~1370%), low-temperature resistance to −25 °C, and heat-accelerated self-healability. Due to its high stretchability, excellent fatigue resistance and high ionic conductivity, the DHB-Fe/CS/PAA can readily work as a stretchable ionic conductor for skin-inspired ionic strain sensor, displaying high sensitivity in a wide strain range (0.5%–500%), fast response time (<180 ms) and excellent durability for 500 cycles at a 100% strain. Besides, the as-assembled ionic sensor is capable of maintaining high ionic conductivity and mechanical robustness at a sub-zero temperature of −25 °C ascribing to the presence of high-concentration charged functional groups and impregnated salts. As a demonstration, a wearable DHB-Fe/CS/PAA ionic sensor in a resistive mode is assembled, demonstrating high sensitivity, wide response range and excellent cyclability in detecting and distinguishing complex human motions rapidly and in real-time.

1. Introduction

Skin-inspired ionic sensor is an emerging wearable sensor by mimicking human skin to realize the perception and response characteristics [1,2]. Ionic sensors have shown high prospects in human-machine interfaces, motion detection and health monitoring, due to their abilities to monitor external stimuli including pressure, strain and torsion rapidly and in real-time [3,4]. Different from the sensors based on measuring the interrogating signals of electrical conductivity, ionic sensors usually possess unique features of high transparency, wide detecting range, and good fitness/wearability [5–7]. However, ionic sensors are highly demanded to endure large deformations of bending, twisting and stretching in their practical applications, putting forward the requirements for high mechanical elasticity of ionic conductors [8]. More importantly, ionic sensors are confronted with poor sensitivity in a wide response range and trade-offs between high mechanical strength and toughness [9,10]. Ionic sensors usually need to withstand cyclic mechanical loadings to adapt to dynamic

* Corresponding author.
** Corresponding author. State Key Laboratory for Modification of Chemical Fibers and Polymer Materials, College of Materials Science and Engineering, Donghua University, Shanghai, 201620, China
E-mail addresses: czhang@dhu.edu.cn (C. Zhang), txliu@fudan.edu.cn (T. Liu).

https://doi.org/10.1016/j.compositesb.2021.108901
Received 22 February 2021; Received in revised form 1 April 2021; Accepted 9 April 2021
Available online 20 April 2021
1359-8368/

environments, inevitably leading to mechanical damages and greatly reduced service life [11]. Therefore, the development of ionic conductors with high mechanical robustness, large stretchability, excellent fatigue resistance and self-healing performance is highly desired.

Ion conductive hydrogels have triggered great attention in the applications of biomedicines and soft robotics, ascribing to a wonderful combination of high mechanical elasticity and excellent ionic conductivity [12–17]. A polyelectrolyte complex hydrogel (PECH) is an emerging ion conductive hydrogel that is derived from a spontaneous association and phase separation of oppositely charged polyelectrolytes in water. The PECH usually demonstrates unique features of high biocompatibility, dynamic reversible electrostatic interactions and high ionic conductivity, showing high potentials as a stretchable ionic conductor for ionic sensors [18]. However, the direct mixing of cationic and anionic polyelectrolytes in water usually leads to serious flocculation, making it difficult to obtain the PECH through direct compounding [18]. The mechanical strengths of PECH are usually one order of magnitude lower than that of human skin, and the poor reversibility of PECH under large deformations and physical damages also limits their practical applications [19]. Besides, the PECH often faces the disadvantages of hydrogel systems with low tolerances to low ambient temperatures, inevitably leading to the loss of mechanical flexibility, ionic conductivity and desirable device performance [20,21]. Although the anti-freezing performance of hydrogels could be enhanced upon the use of glycol-based agents, these anti-freezing agents among the PECH would inevitably bring about biological toxicity and environmental hazards together with significantly reduced ionic conductivity [22]. Therefore, the development of the PECH simultaneously engaging high mechanical elasticity, high biocompatibility, and decent freeze-resistant properties presents significant prospects while challenging.

Herein, a highly stretchable, fatigue-resistant and self-healable ion conductive hydrogel is fabricated by a hydrogen-bonded network densification strategy, which is consisted of two steps. First, a double-networked hydrogel (Fe/CS/PAA) was prepared through a hydrogel network-constrained polymerization, during which an anionic Fe^{3+}-coordinated polyacrylic acid network (Fe-PAA) was in-situ formed in a confined space of a cationic Fe^{3+}-coordinated chitosan network (Fe-CS) due to strong electrostatic interactions. Second, a densified hydrogen-bonded network between the Fe-PAA and Fe-CS chains activated by salt impregnation was achieved for fabricating a densified hydrogen-bonded Fe/CS/PAA (DHB-Fe/CS/PAA), which exhibits high tensile strength of ~0.34 MPa, large stretchability of >1370%, and excellent fatigue resistance for 1000 cycles. Owing to the abundant charged groups and impregnated salts, the DHB-Fe/CS/PAA demonstrates high ionic conductivity of 0.24 S m^{-1} and excellent mechanical flexibility tolerant to a subzero temperature of −25 °C. Benefiting from its high stretchability, excellent fatigue resistance, high ionic conductivity and excellent self-healing performance (healing efficiency of ~70%), the DHB-Fe/CS/PAA ionic sensor shows stable resistance signals in a wide strain range of 0.5%–500%, fast response time of <180 ms, and excellent durability at a 100% strain for 500 cycles. As a proof of concept, a wearable DHB-Fe/CS/PAA ionic sensor is assembled, achieving real-time monitoring of complex human motions including swallowing, finger bending and wrist bending. This study might provide a new path for the development of ion conductive hydrogels with excellent mechanical elasticity, high ionic conductivity, self-healability and low-temperature tolerance for next-generation ionic skin sensors.

2. Experimental section

2.1. Preparation of hydrogel samples of Fe/CS/PAA and DHB-Fe/CS/PAA

In a typical procedure, 1 g of acrylic acid (AA), designed amounts of $FeCl_3{\cdot}6H_2O$ and CS were dissolved in 4 mL of 2% acetic acid solution. Upon dissolution, 10 mg of ammonium persulfate (APS) was added to the above solution under stirring. The mixed solution was diluted to 5 mL with 2% acetic acid solution, degassed in a vacuum, cast into a poly (tetrafluoroethylene) (PTFE) mold, and subsequently heated at 70 °C for 12 h, producing hydrogel samples denoted as Fe/CS/PAA. To clearly show the compositions of these hydrogel samples, synthetic details and abbreviation naming rules were summarized in Table 1. Typically, the Fe1/CS1/PAA20, Fe2/CS1/PAA20, Fe3/CS1/PAA20 and Fe4/CS1/PAA20 represent the resultant hydrogel samples at a $FeCl_3{\cdot}6H_2O$/AA weight ratio of 0.05, 0.10, 0.15 and 0.20, respectively, while keeping the concentrations of AA and CS at 200 and 10 mg mL^{-1}, respectively. The Fe2/CS0.5/PAA20, Fe2/CS1.5/PAA20 and Fe2/CS2/PAA20 represent the resultant hydrogel samples with the initial concentrations of CS at 5, 15, and 20 mg mL^{-1}, respectively, while keeping the concentrations of AA and $FeCl_3{\cdot}6H_2O$ at 200 and 20 mg mL^{-1}, respectively. For comparison, hydrogel sample of Fe/PAA was prepared according to the procedure of Fe2/CS1/PAA20 in the absence of CS. Hydrogel sample of PAA was prepared according to the above steps for the synthesis of Fe/PAA except for the absence of $FeCl_3{\cdot}6H_2O$. To be specially noted, a simple CS solution or CS solution containing iron ions cannot form hydrogels. The as-obtained hydrogel samples of Fe/CS/PAA were immersed in saturated NaCl solution for 1 h and aged for another 12 h to produce the DHB-Fe/CS/PAA with sample names prefixed of "DHB-" before corresponding hydrogel samples of Fe/CS/PAA and Fe/PAA.

2.2. Characterizations

Chemical compositions and interactions of freeze-dried hydrogel samples were analyzed by Fourier transform infrared (FTIR) in a frequency range of 600–4000 cm^{-1} in an attenuated total reflection (ATR) mode (Nicolet 6700). Morphologies and microstructures of freeze-dried hydrogel samples were characterized using field-emissions scanning electron microscopy (FESEM, Ultra 55). Viscoelasticity of hydrogel samples was investigated by a rheometer (Anton Paar MCR301) at room temperature. Storage modulus (G′) and loss modulus (G″) were recorded at a strain and frequency of 1%–1000% and 1 rad s^{-1}, respectively, in a strain sweep measurement. Oscillatory frequency sweep measurements were carried out to determine the G′ and G″ over a shearing frequency range from 0.1 to 100 rad s^{-1} at a 1% strain. Mechanical properties of hydrogel samples were performed on a universal testing machine (UTM2102, SUNS). Cylindrical hydrogel samples (diameter: 15 mm; height: 20 mm) were prepared for compressive measurements. Rectangular hydrogel samples (50 × 5 × 2 mm^3) were prepared and stretched at a speed of 20 mm min^{-1} for tensile tests. Samples were loaded at a speed of 20 mm min^{-1} at 25 and -25 °C, respectively. Silicone oil was used to cover hydrogel samples to prevent the evaporation of water during mechanical tests. Measurements of ionic conductivity were

Table 1
Synthetic details for hydrogel samples of Fe/CS/PAA.

Sample names	AA (mg mL^{-1})	$FeCl_3{\cdot}6H_2O$ (mg mL^{-1})	CS (mg mL^{-1})	Sample names after salt impregnation
Fe1/CS1/PAA20	200	10	10	DHB-Fe1/CS1/PAA20
Fe2/CS1/PAA20	200	20	10	DHB-Fe2/CS1/PAA20
Fe3/CS1/PAA20	200	30	10	DHB-Fe3/CS1/PAA20
Fe4/CS1/PAA20	200	40	10	DHB-Fe4/CS1/PAA20
Fe2/CS0.5/PAA20	200	20	5	DHB-Fe2/CS0.5/PAA20
Fe2/CS1.5/PAA20	200	20	15	DHB-Fe2/CS1.5/PAA20
Fe2/CS2/PAA20	200	20	20	DHB-Fe2/CS2/PAA20
Fe/PAA	200	20	0	DHB-Fe/PAA
PAA	200	0	0	–

carried out by electrochemical impedance spectroscopy (EIS) at room temperature on an electrochemical workstation (CHI 660D, Shanghai Chenhua). Hydrogel samples were sandwiched between two gold-plated electrodes, and ionic conductivities (σ) of hydrogel samples were estimated using the following equation:

$$\sigma = \frac{L}{R_b \times S}$$

where L is the distance between electrodes, R_b is the bulk resistance of hydrogels, and S is the contacting area of the hydrogel sample with electrodes.

Hydrogel samples were cut into two halves using a blade for evaluating their self-healing performance. One-half of hydrogel samples were dyed with phthalocyanine green for a visual discrimination purpose, after which separated hydrogels with a fresh surface were brought into close contact. During the self-healing process, hydrogel samples were covered with silicone oil, stored in a polyethylene sealed bag, and placed at room temperature or in an oven at 70 °C for certain time. Healing efficiency (HE) of hydrogel samples was evaluated by the recovery of tensile strengths after cutting and self-healing, which was calculated by the following equation [23,24]:

$$HE = \frac{\sigma'}{\sigma} \times 100\%$$

where σ and σ' are tensile strengths of hydrogel samples before and after cutting and self-healing. The recovery of hydrogel samples in ionic conductivity was demonstrated by lighting up a light-emitting diode (LED) during the cutting and self-healing processes.

2.3. Measurements of ionic resistance sensors

Ionic resistance sensing measurements were carried out by a combination of tensile and resistance tests. Resistive signals were recorded with a SourceMeter (2612B, Keithley) and strain data was recorded by a universal testing machine (UTM2102, SUNS). Relative resistance changes of hydrogel samples were calculated as follows:

$$\frac{\Delta R}{R_0} = \frac{R - R_0}{R_0}$$

where R_0 and R represent the initial and dynamic resistances, respectively.

Ionic sensor was assembled by using one piece of hydrogel samples sandwiched between two pieces of VHB tapes. The as-fabricated sensor was attached to the throat, finger, opisthenar, wrist, elbow joint, and knee of a volunteer, and real-time R-t curves were recorded at room and low temperatures, respectively.

3. Results and discussion

3.1. Fabrication and structural characterizations of DHB-Fe/CS/PAA

A hydrogen-bonded network densification strategy is presented for preparing the target DHB-Fe/CS/PAA (Fig. 1a). During the hydrogen-bonded network densification, free-radical polymerization of AA was achieved within a confined space of polyelectrolyte network skeleton of cationic Fe-CS networks due to electrostatic interactions, obtaining transparent orange hydrogel samples of Fe/CS/PAA. This process ensured molecularly compounding of anionic Fe-PAA and cationic Fe-CS networks, effectively preventing any possible flocculation. After this, the introduction of high-concentration salts destroyed the ion complexation between the two hydrogel networks of Fe-PAA and Fe-CS to a certain extent and significantly led to the formation of dense hydrogen-bonded interactions between the two networks on the premise of ensuring their uniform recombination. Three aims were realized concurrently through the salt impregnation: (1) Inorganic salts endowed the resultant DHB-

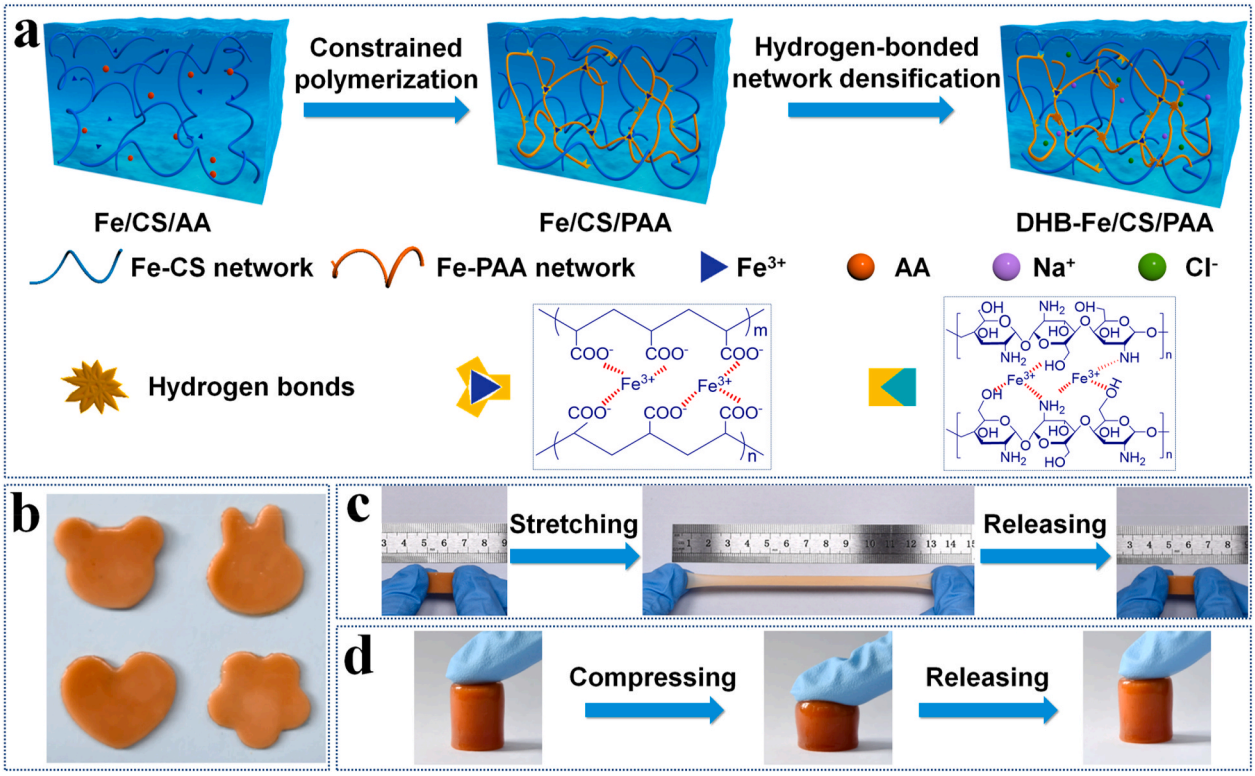

Fig. 1. Preparation and schematic of the DHB-Fe/CS/PAA. (a) Schematic illustration of the preparation procedures of DHB-Fe/CS/PAA through hydrogel network-constrained polymerization and hydrogen-bonded network densification processes. (b) Photograph showing hydrogel samples of DHB-Fe2/CS1/PAA20 in various shapes. Photographs showing hydrogel samples of DHB-Fe2/CS1/PAA20 under (c) stretching/releasing and (d) compressing/releasing processes.

Fe/CS/PAA with anti-freezing properties [25]; (2) Inorganic salts endowed the resultant DHB-Fe/CS/PAA with largely enhanced ionic conductivity; (3) Inorganic salts induced the oppositely charged hydrogel networks with high electrostatic repulsions, which are conducive to the effective entanglement between hydrogel networks and the enhancement of dense hydrogen-bonded interactions [26,27]. As a result, a transparent Fe/PAA/CS turned into opaque DHB-Fe/CS/PAA (Fig. S1), ascribing to the formation of a dense hydrogen-bonded network [28,29]. The hydrogen bond network densification strategy is simple and feasible, which is very easy to construct DHB-Fe/CS/PAA with complex shapes (Fig. 1b).

The DHB-Fe2/CS1/PAA20 samples can be stretched/compressed and instantaneously recovered to its original shape after removing the external force (Fig. 1c and d), indicating that the DHB-Fe2/CS1/PAA20 possessed an outstanding recovery performance. A comparison sample of One-Pot-Fe2/CS1/PAA20 was produced by in-situ polymerization of the aqueous solution containing CS, AA, $FeCl_3{\cdot}6H_2O$, and NaCl in one-pot. The as-prepared One-Pot-Fe2/CS1/PAA20 showed poor elastic recovery performance (Fig. S2), low tensile strength and unsatisfying elongation at break (Fig. S3). During the deformation, the dense hydrogen-bonded interactions served as "sacrifice bonds" to consume energy [30], contributing to the outstanding mechanical performance of DHB-Fe/CS/PAA.

Surface morphologies of freeze-dried hydrogel samples of Fe/PAA, Fe/CS/PAA and DHB-Fe/CS/PAA were investigated to investigate the crosslinking density among the DHB-Fe/CS/PAA. The Fe/PAA exhibited a typical 3D interconnected network with a relatively uniform macroporous structure (Fig. 2a). With the incorporation of Fe/PAA network into the confined space of Fe/CS network, the pore sizes among the Fe/CS/PAA largely decreased (Fig. 2b). Compared with the Fe/CS/PAA, the microstructure of DHB-Fe/CS/PAA became compact (Fig. 2c). These structural changes were mainly attributed to the formation of a dense hydrogen-bonded network that led to high-degree entanglements of polymer chains, which were conducive to high stretchability and large deformation-tolerant performance of DHB-Fe/CS/PAA. To demonstrate the existence of coordination interactions and dense hydrogen bonds, FTIR spectra were conducted to characterize the chemical structures of CS, PAA, Fe/PAA, Fe/CS/PAA and DHB-Fe/CS/PAA. The band at 1694 cm^{-1} represented the C═O symmetrical stretching vibration of PAA and a blue shift that occurred in Fe/PAA (1709 cm^{-1}) was caused by the formation of ion coordination interactions (Fig. 2d) [28,31]. The bands at 1644 cm^{-1} and 1587 cm^{-1} (Fig. 2e) were assigned to stretching vibrations of C═O in primary amine and the bending vibration of N–H in $–NH_2$ groups, respectively [31]. The bands of CS at 1644 cm^{-1} and 1587 cm^{-1} disappeared in the DHB-Fe/CS/PAA (Fig. 2f), indicating that hydrogen-bonded interactions between the Fe/PAA and Fe/CS networks were formed [32,33]. The band assigned to C═O stretching vibration shifted from 1709 to 1699 cm^{-1} in the Fe/CS/PAA (Fig. 2g), indicating the formation of hydrogen bonds between Fe/CS and Fe/PAA chains. After the salt impregnation process, the absorption band of C═O

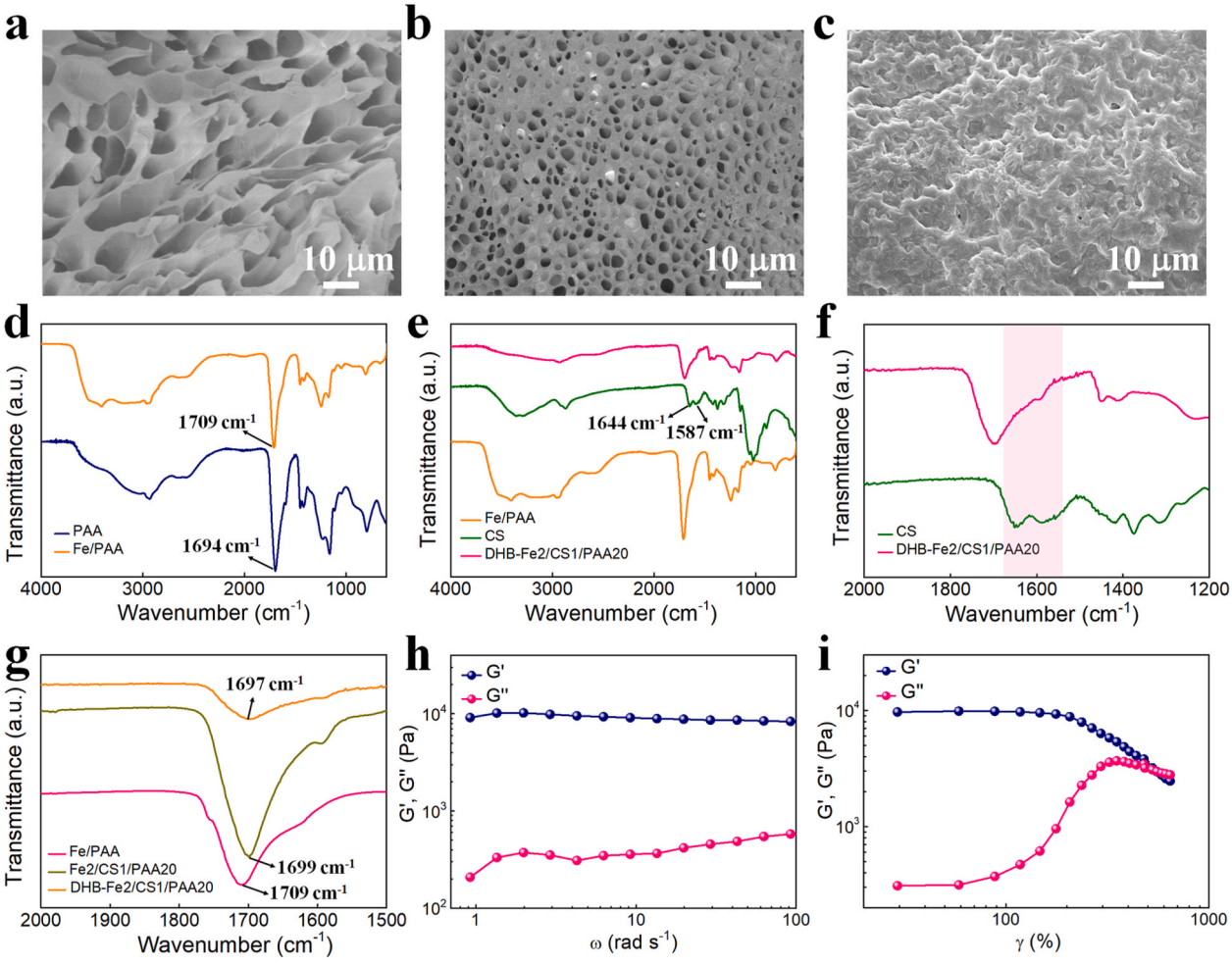

Fig. 2. Structural and compositional characterizations of the PECH. SEM images of freeze-dried hydrogel samples of (a) Fe/PAA, (b) Fe2/CS1/PAA20 and (c) DHB-Fe2/CS1/PAA20. (d) ATR-IR spectra of PAA and Fe/PAA. (e) ATR-IR spectra of Fe/PAA, CS and DHB-Fe2/CS1/PAA20. Enlarged ATR-IR spectra of (f) CS and DHB-Fe2/CS1/PAA20 in a wavenumber range of 1200–2000 cm^{-1}, (g) Fe/PAA, Fe2/CS1/PAA20 and DHB-Fe2/CS1/PAA20 in a wavenumber range of 1500–2000 cm^{-1}. (h) Oscillatory frequency sweep test at a shear strain of 1% and (i) oscillatory amplitude sweep test at an angular frequency of 1 rad s^{-1} for DHB-Fe2/CS1/PAA20.

stretching of DHB-Fe/CS/PAA slightly shifted from 1699 to 1697 cm^{-1}, attributed to the strengthening of intramolecular and intermolecular hydrogen bond interactions. The strengthening of hydrogen bond interactions reduced the force constants of C═O chemical bonds, leading to red shifting of vibrational frequencies to low wavenumbers [34].

Dynamic rheological measurements were carried out to reveal viscoelastic properties of DHB-Fe/CS/PAA. The frequency dependence of viscoelastic characteristics was observed by oscillation frequency sweep test under a small shear strain (Fig. 2h). The storage modulus (G′) of DHB-Fe2/CS1/PAA20 was much higher than its loss modulus (G″) in the angular frequency range of 1–100 rad s^{-1}, indicating an elastic nature of the DHB-Fe/CS/PAA [35,36]. In strain sweep measurements, the DHB-Fe2/CS1/PAA20 was endowed with high G′, and the G″ value was less than that of G′ in a certain region ($\gamma < 550\%$) (Fig. 2i), indicating that the DHB-Fe/CS/PAA exhibited an elastic feature. The G′ value was crisscrossed with the G″ value at a shear frequency of 550%, due to the collapse of the hydrogel network inside the DHB-Fe/CS/PAA [37]. These results discussed above demonstrated the viscoelasticity and toughness of the DHB-Fe/CS/PAA.

3.2. Mechanical properties of DHB-Fe/CS/PAA

Ion conductive hydrogels with robust mechanical strength and toughness are highly required for meeting the complex deformation requirements of ionic sensors [38]. Mechanical properties of Fe/PAA, DHB-Fe/PAA, Fe/CS/PAA and DHB-Fe/CS/PAA were investigated by tensile measurements. The Fe/CS hydrogel network cannot even be tested by tensile tests because it is not self-supporting (Fig. S4). After the as-prepared hydrogels were placed for various time, the mechanical and electrical properties of hydrogel samples were largely affected due to the evaporation of water (Fig. S5). Therefore, hydrogel samples were covered with silicone oil to prevent any evaporation of water during long-term mechanical tests. The Fe/PAA exhibited a low tensile strength of 0.03 MPa and elongation at break of 620% (Fig. 3a). When the density of hydrogen-bonded network increased by salt impregnation, tensile strength and elongation at break of DHB-Fe/PAA increased simultaneously. Interestingly, mechanical properties of Fe2/CS1/PAA20 dramatically increased once the dense hydrogen-bonded network was formed between the carboxyl groups of Fe/PAA and the amino groups of Fe/CS. In contrast, the DHB-Fe2/CS1/PAA20 displayed largely enhanced mechanical strength and toughness compared with those of Fe/PAA, DHB-Fe/PAA and Fe/CS/PAA. The strengthening and toughening mechanisms were proposed as follows: First, the salting-out effect decreased the water contents of DHB-Fe/CS/PAA, which directly increased the density of the hydrogen-bonded network. Second, the wrinkled microstructures due to the shrinkage of polymer chains during salt impregnation enabled the DHB-Fe/CS/PAA with high toughness similar to the functions of hidden lengths [39]. Third, the formation of Fe/CS chain entanglements in DHB-Fe/CS/PAA was also the reason for toughness enhancement.

By tuning the weight ratio of $FeCl_3{\cdot}6H_2O$/AA, a series of DHB-Fe/CS/PAA with tailored mechanical properties were obtained (Fig. 3b). When

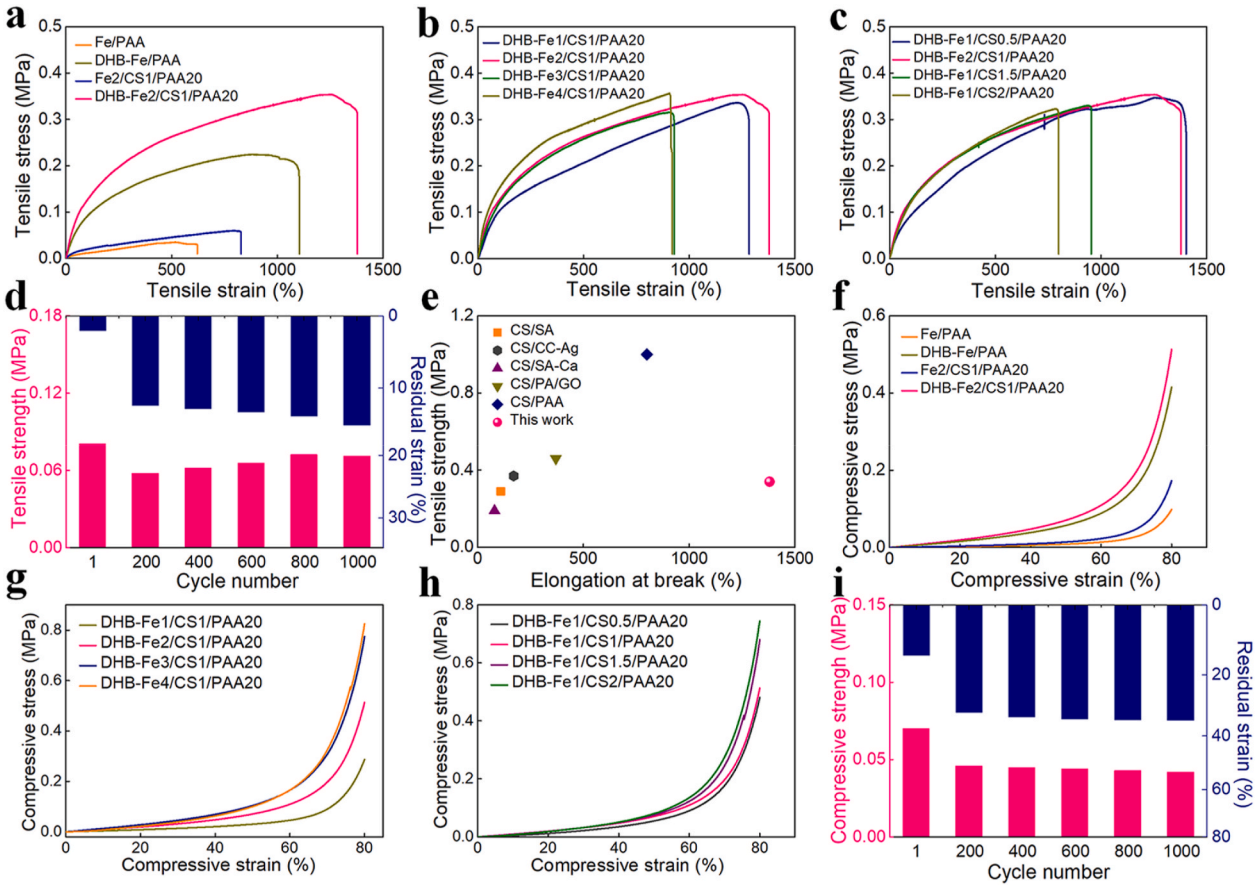

Fig. 3. Mechanical properties of the DHB-Fe/CS/PAA. (a) Tensile stress-strain curves of Fe/PAA, DHB-Fe/PAA, Fe2/CS1/PAA20 and DHB-Fe2/CS1/PAA20. Tensile stress-strain curves of DHB-Fe/CS/PAA with various contents of (b) $FeCl_3{\cdot}6H_2O$ and (c) CS. (d) Tensile strength and residual strain of DHB-Fe2/CS1/PAA20 after various cycles of successive loading-unloading at a tensile strain of 50%. (e) Comparisons of tensile strength and elongation at break of various PECH samples in literature. (f) Compressive stress-strain curves of Fe/PAA, DHB-Fe/PAA, Fe2/CS1/PAA20 and DHB-Fe2/CS1/PAA20. Compressive stress-strain curves of DHB-Fe/CS/PAA with various contents of (g) $FeCl_3{\cdot}6H_2O$ and (h) CS. (i) Compressive strength and residual strain of DHB-Fe2/CS1/PAA20 after various cycles of successive loading-unloading at a compressive strain of 50%.

increasing the weight ratio of $FeCl_3{\cdot}6H_2O$/AA up to 0.1, the DHB-Fe2/CS1/PAA20 exhibited high elongation at break of ~1370% and high tensile strength of ~0.34 MPa. It explained that an appropriate loading of $FeCl_3{\cdot}6H_2O$ increased the cross-linking points of DHB-Fe/CS/PAA, contributing to improved mechanical properties [40]. However, further increases in the weight ratio to 0.2 decreased the stretchability of DHB-Fe/CS/PAA. The excess amount of $FeCl_3{\cdot}6H_2O$ further increased the cross-linking points, rendering densely cross-linked Fe/PAA and Fe/CS networks with decreased elongation at break [41]. Since the Fe/CS network could interact with Fe/PAA network through hydrogen-bonded interactions, the CS concentration had a great influence on the mechanical performance of DHB-Fe/CS/PAA. An increase in the concentration of CS increased the mechanical fracture strain of DHB-Fe/CS/PAA (Fig. 3c). The DHB-Fe2/CS1/PAA20 with 10 mg mL^{-1} of CS provided high fracture strain and toughness, because the density of hydrogen-bonded network gradually increased with the increase of CS. As the concentration of CS continually increased, the elongation at break of DHB-Fe/CS/PAA gradually decreased, explaining that the rigid nature of CS chains might partially impair the flexibility of DHB-Fe/CS/PAA. The 1000 successive stretching-releasing cycles were performed at a fixed strain of 50% on DHB-Fe2/CS1/PAA20 to evaluate the recovery performance (Figs. 3d and S6a). The tensile strength of DHB-Fe2/CS1/PAA20 increased slightly due to an inevitable evaporation of water during the fatigue tests. Only 15.5% of a residual strain remained after 1000 consecutive tensile loading-unloading cycles, showing its excellent self-recovery performance. The tensile strength and elongation at break of PECH samples including chitosan/sodium alginate (CS/SA) [18], chitosan/carboxymethyl chitosan/AgNPs (CS/CC-Ag) [42], chitosan/sodium alginate/calcium ion (CS/SA-Ca) [43], chitosan/polyacrylate/graphene oxide (CS/PA/GO) [32], and chitosan/poly(acrylic acid) (CS/PA) [44] were summarized and compared with this study (Fig. 3e). We comment that the resultant DHB-Fe/CS/PAA indicates higher tensile strength and tensile strain than those of PECH in literature.

To better understand the reinforcement of mechanical properties of DHB-Fe/CS/PAA by the dense hydrogen-bonded network, uniaxial compression tests of Fe/PAA, DHB-Fe/PAA, Fe/CS/PAA and DHB-Fe/CS/PAA were performed. The results demonstrated that incorporating the dense hydrogen-bonded interactions greatly improved the compression strength of DHB-Fe2/CS1/PAA20 (Fig. 3f), which was consistent with its tensile results. A variety of DHB-Fe/CS/PAA with diverse weight ratios of $FeCl_3{\cdot}6H_2O$/AA and various CS concentrations were compressed under a raising strain. The compression strength of DHB-Fe/CS/PAA increased apparently with an increasing weight ratio of $FeCl_3{\cdot}6H_2O$/AA from 0.05 to 0.2 (Fig. 3g), attributed to an increasing coordination interaction and enhanced hydrogen-bonded network. With the increase of CS concentration from 5 to 20 mg mL^{-1}, the compression strength of DHB-Fe/CS/PAA at an 80% strain increased from 0.48 to 0.74 MPa (Fig. 3h), implying the contribution of dense hydrogen bonds to the mechanical properties. These results indicated that the trade-offs between the mechanical parameters were achieved by simply adjusting the contents of each component. Furthermore, fatigue resistance tests of DHB-Fe2/CS1/PAA20 were carried out under repeated compression cycles at a 50% strain (Figs. 3i and S6b). An obvious hysteresis was observed in the first cycle, and hysteresis loops generally became small upon increasing the cycling number. The DHB-Fe2/CS1/PAA20 had an effective energy dissipation due to the fracture of extensive intermolecular hydrogen bonds and the dis-entanglement of network chains. As the cycling number continually increased, the DHB-Fe2/CS1/PAA20 retained a non-recoverable deformation, indicating that the destruction of the hydrogel network was the leading factor for dissipating energy.

3.3. Conductivity properties and anti-freezing performance of DHB-Fe/CS/PAA

It is well known that high conductivity is beneficial for ionic skin sensors. The existence of free ions in networks, such as Cl^- and Na^+ ions, contributed to the high ionic conductivity of DHB-Fe2/CS1/PAA20. The ionic conductivity of DHB-Fe2/CS1/PAA20 was measured by EIS (Fig. S7a). In the high-frequency region of Nyquist plots, the semicircular pattern indicates the charge transfer resistance (R_{ct}) (Fig. S7b) [45]. The DHB-Fe2/CS1/PAA20 showed a markedly small R_{ct}, signifying that ions had a small barrier to move or diffuse in the hydrogel network. By calculating from the R_{ct}, the DHB-Fe2/CS1/PAA20 obtained high ionic conductivity of 0.24 S m^{-1}, making it promising to act for ionic sensors. Variations in resistance of DHB-Fe2/CS1/PAA20 following applied strains could be tracked by directly connecting it to a digital multimeter (Fig. 4a). As the hydrogel was stretched, the brightness of the light-emitting diode (LED) gradually decreased because of increased resistance, indicating the feasibility of the deformable DHB-Fe2/CS1/PAA20 as a strain sensing platform. The resistance of DHB-Fe2/CS1/PAA20 significantly increased with the increase of strain (Fig. 4b), providing an opportunity to convert mechanical deformation into detectable electrical signals.

In general, conventional ionic sensors inevitably freeze and lose their conductivity at low temperatures, which severely limits their practical applications at sub-zero temperatures. NaCl solution has a lower freezing point than that of pure water because of the colligative property for a diluted salt solution [46]. The freezing point of DHB-Fe2/CS1/PAA20 decreased due to the interaction between the Na^+/Cl^- ions and water molecules [47]. To evaluate the mechanical performance of DHB-Fe/CS/PAA at sub-zero temperatures, the Fe2/CS1/PAA20 and DHB-Fe2/CS1/PAA20 were placed in a cryogenic refrigeration circulator (−25 °C) for 2 h. Unlike the case of Fe2/CS1/PAA20, the anti-freezing DHB-Fe2/CS1/PAA20 could illuminate a LED lamp even at −25 °C (Fig. 4c) whereas the Fe2/CS1/PAA20 failed (Fig. 4d). Moreover, the DHB-Fe2/CS1/PAA20 showed excellent bending flexibility (Fig. 4e), while the Fe2/CS1/PAA20 easily abandoned its mechanical flexibility, and brittle fracture occurred easily when bending at subzero temperatures (Fig. 4f), indicating the excellent anti-freezing performance of DHB-Fe2/CS1/PAA20 (Fig. 4g and 4h). To systematically evaluate the anti-freezing performance of DHB-Fe/CS/PAA, tensile properties at various temperatures were carried out by an electronic universal testing machine equipped with an environmental chamber. Stress-strain curves of DHB-Fe2/CS1/PAA20 at various temperatures illustrated that the tensile strength increased significantly and the elongation at break decreased rapidly (Fig. 4i), indicating the improvement of rigidity and weakness of extensibility at sub-zero temperatures. Even at −30 °C, the DHB-Fe2/CS1/PAA20 remained deformable and stretchable to 220%. The mechanical flexibility of DHB-Fe2/CS1/PAA20 at low temperatures revealed its prominent anti-freezing performance. The stable mechanical flexibility and ion conductive properties of anti-freezing DHB-Fe/CS/PAA made it an ideal candidate for ionic skin sensors in extremely low sub-zero temperatures.

3.4. Self-healing performance of DHB-Fe/CS/PAA

The DHB-Fe/CS/PAA incorporated with self-healing properties can significantly improve the durability of ionic skin sensors and extend the corresponding lifetime for practical applications [48–51]. Benefiting from the dynamic and reversible hydrogen-bonded network and metal coordination interactions, the DHB-Fe2/CS1/PAA20 exhibited an excellent self-healing property both in mechanical and conductive performance. An intact DHB-Fe2/CS1/PAA20 was cut into two segments, and one of the pieces was dyed green with phthalocyanine green (Fig. 5a). The separate halves with different colors were brought into intimate contact and then sealed in a polyethylene bag at 70 °C to

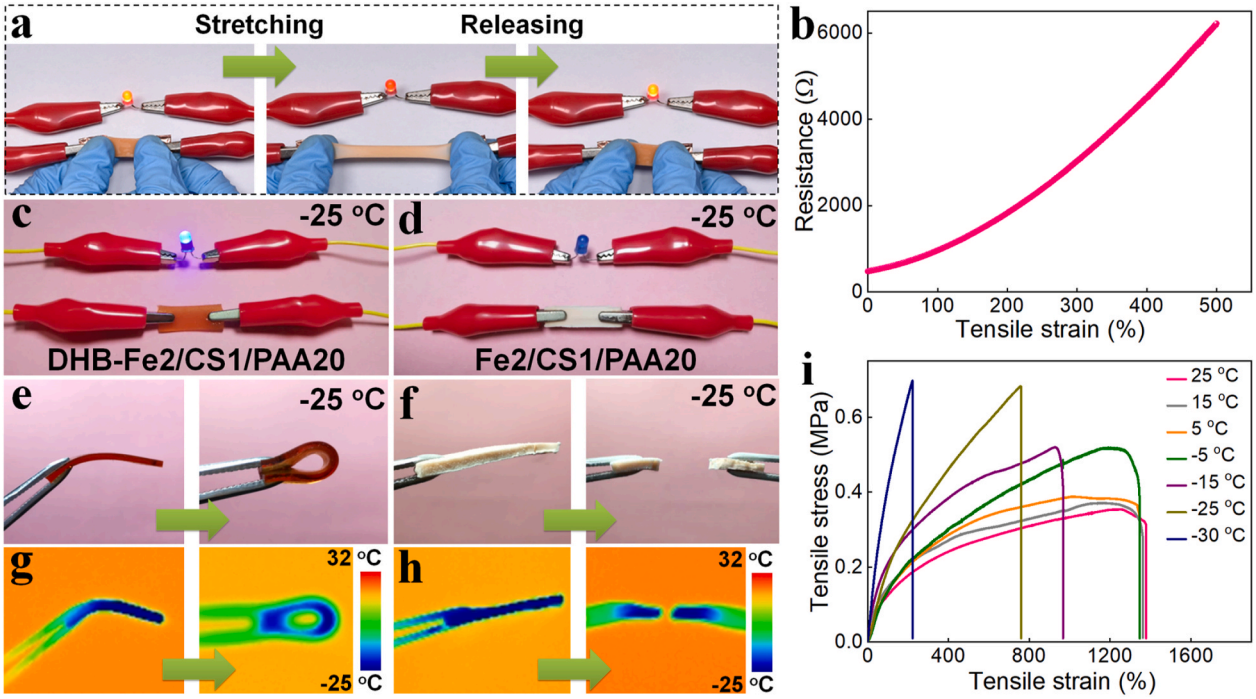

Fig. 4. Ionic conductivity and anti-freezing performance of the DHB-Fe/CS/PAA. (a) Photographs showing high ionic conductivity of DHB-Fe2/CS1/PAA20 under stretching/releasing processes. (b) Resistance variations of DHB-Fe2/CS1/PAA20 under stretching. Photographs showing (c) DHB-Fe2/CS1/PAA20 and (d) Fe2/CS1/PAA20 connected to a circuit to lighten up a bulb at −25 °C. Bending of (e) DHB-Fe2/CS1/PAA20 and (f) Fe2/CS1/PAA20 at −25 °C. Infrared images of (g) DHB-Fe2/CS1/PAA20 and (h) Fe2/CS1/PAA20 at −25 °C. (i) Tensile stress-strain curves of DHB-Fe2/CS1/PAA20 at various temperatures.

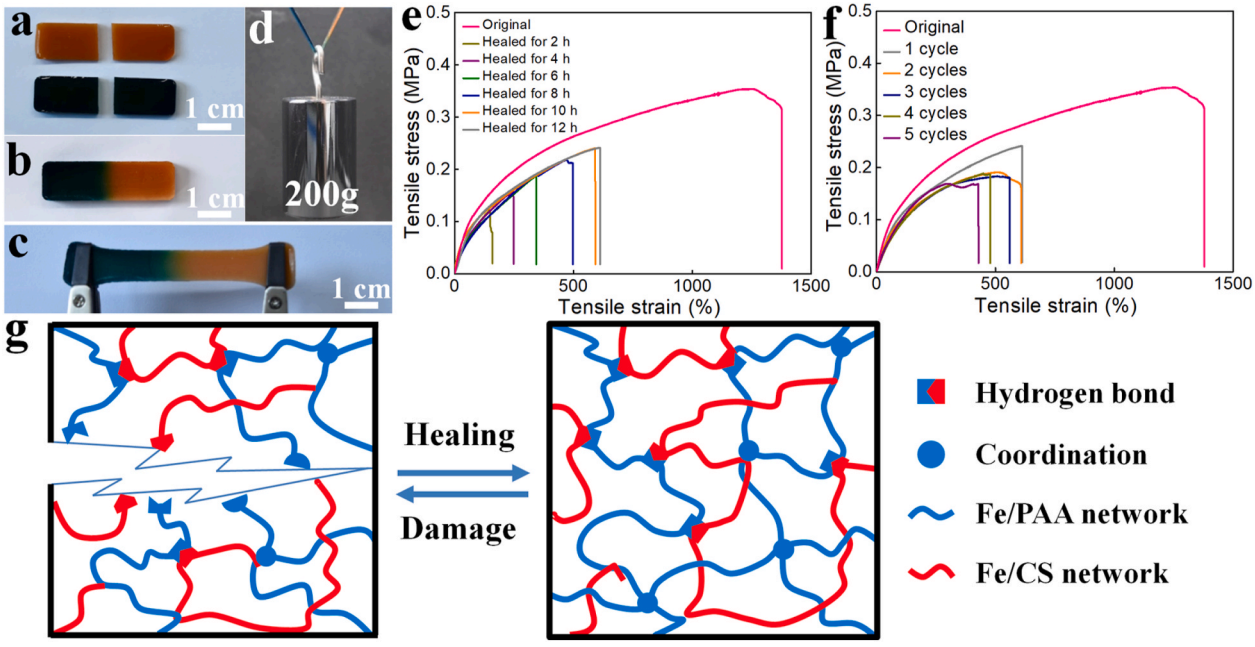

Fig. 5. Self-healing performance of the DHB-Fe/CS/PAA. (a) Photographs showing the DHB-Fe2/CS1/PAA20 that was dyed and cut into pieces. (b) Photographs showing the self-healed DHB-Fe2/CS1/PAA20. Photographs showing the self-healed DHB-Fe2/CS1/PAA20 (c) being stretched and (d) holding a weight of 200 g. (e) Tensile stress-strain curves of DHB-Fe2/CS1/PAA20 after cutting and self-healing for various healing time. (f) Tensile stress-strain curves of DHB-Fe2/CS1/PAA20 after multiple cutting/self-healing cycles. (g) Schematic illustration of the self-healing process of DHB-Fe/CS/PAA.

achieve complete healing from damages (Fig. 5b). After healing for 12 h, the healed DHB-Fe2/CS1/PAA20 could be stretched without breaking the healed crack (Fig. 5c). The healed DHB-Fe2/CS1/PAA20 is capable of holding a weight of 200 g (Fig. 5d), confirming the reliable self-healing properties of fractured DHB-Fe2/CS1/PAA20. The self-healing ability of ionic conductivity was studied by recording the brightness variations of an LED bulb in the circuit during cutting/healing processes (Fig. S8a). When the DHB-Fe2/CS1/PAA20 was cut into two pieces, the resulting open circuit would cause an immediate extinction of the LED bulb. The LED bulb was turned on again after healing. The self-healing properties of DHB-Fe2/CS1/PAA20 were quantitatively studied by tensile tests. Tensile strength of the healed

DHB-Fe2/CS1/PAA20 increased with the healing time (Fig. 5e). The healing efficiency reached almost 70% after 12 h (Fig. S8b), due to the increased mobility of ferric ions and polymer chains in these hydrogels over a long time. Successive cutting and healing steps were carried out on the same hydrogels. Moreover, the healing took place even after the fourth rupture (Fig. 5f), exhibiting a long lifetime.

The fracture tensile strength and elongation at break of the DHB-Fe2/CS1/PAA20 samples that were cut and self-healed at room temperature for 24 h were 0.10 MPa and 195%, respectively (Fig. S9a). The healing efficiency of hydrogel samples healed at room temperature was only 30% (Fig. S9b) due to the dense hydrogen-bonded network structure made chain motions slowly. Taking the self-healing efficiency into consideration, the healing temperature of DHB-Fe2/CS1/PAA20 was set at 70 °C. A possible mechanism was proposed to elucidate the self-healing performance of DHB-Fe/CS/PAA (Fig. 5g). When the DHB-Fe/CS/PAA was cut into separate parts, the physical interactions including hydrogen bonds and ionic coordination were destroyed. When the two segments were put together, the dynamic interactions between Fe^{3+} and –COOH functional groups caused ferric ions to migrate from one side to the other, leading to hydrogel healing. Furthermore, hydrogen bonds between Fe/CS and Fe/PAA chains also contributed to an improvement of the self-healing property. In this way, the DHB-Fe/CS/PAA on the fracture surfaces could reconstruct ionic coordination interactions and hydrogen bonds, thus enabling the fractured hydrogel to be well healed.

3.5. Strain sensing performance of DHB-Fe/CS/PAA ionic sensors

Integration of excellent ionic conductivity, high stretchability and excellent resilience in the DHB-Fe/CS/PAA makes it a promising candidate for the fabrication of flexible electronics, especially ionic strain sensors. During the tensile loading-unloading processes, the resistance of DHB-Fe2/CS1/PAA20 changed accordingly, which made DHB-Fe2/CS1/PAA20 an ionic skin material for resistive-type strain sensors by converting mechanical deformation into detectable electrical signals. After being encapsulated, the DHB-Fe2/CS1/PAA20 was connected to a conductor characterization system to assess its conductivity response. The relative resistance signals showed incremental responses under the strain ranging from 0.5% to 500% in successive tests (Figs. 6a and S10a). The ionic strain sensors generated highly reversible and reproducible $\Delta R/R_0$ signals during the repeated stretching-releasing cycles, suggesting their high sensitivity and reliability by detecting a wide range of strains. To investigate the stability of DHB-Fe2/CS1/PAA20 ionic sensors to small- and large-strain deformation, six cycles of 0.5 and 500% strains were tested respectively (Figs. 6b and S10b). The relative resistance changes of the ionic sensors were stable under loading-unloading cycles without obvious hysteresis under both small and large strains, demonstrating the wide-range strain sensing capability of DHB-Fe2/CS1/PAA20. The relative resistance changes increased linearly upon the applied strain (Fig. 6c). Gauge factor (GF), which is an important parameter for evaluating the sensitivity of strain sensor, can be defined as the slope of resistance changes versus applied stress [52]. It could be found that the GF was not a constant value in the whole strain window. The GF value of the DHB-Fe2/CS1/PAA20 sensor was 1.4 and 2.2 in the strain range of 0–100% and 100–300%, respectively. The GF value rose to 3.1 within a high strain (300–500%), indicating better sensitivity at high deformation. Cycling stability is a vital property for the long-term service of ionic sensors. The DHB-Fe2/CS1/PAA20 maintained an initial amplitude of resistance change even after ~500 stretching/releasing cycles at a strain of 100% (Fig. S10c), strongly

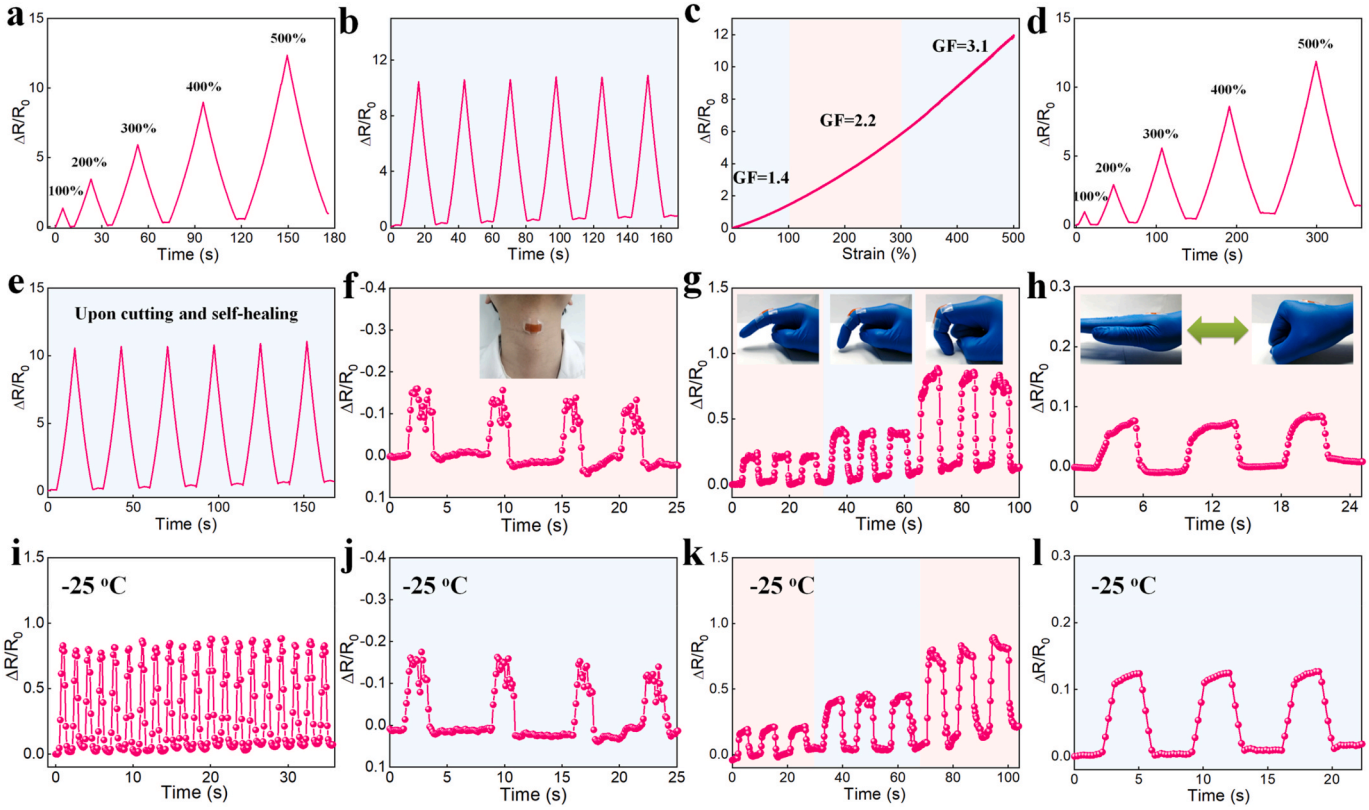

Fig. 6. Resistive sensing performance of DHB-Fe2/CS1/PAA20 ionic sensors. Relative resistance changes under (a) various strains and (b) a large strain of 500% for 6 cycles. (c) Relative resistance variations under various strains. Relative resistance changes of the healed DHB-Fe2/CS1/PAA20 under (d) various strains and (e) a large strain of 500% for 6 cycles. Relative resistance variations for monitoring real-time human motions of (f) swallowing, (g) finger bending, (h) opisthenar bending. (i) Relative resistance changes under repeated stretching-releasing cycles under a 50% strain at −25 °C. (j) Relative resistance changes for monitoring saliva swallowing at −25 °C. Relative resistance changes monitoring (k) finger and (l) opisthenar bending at −25 °C.

confirming the excellent conductivity stability and reproducibility for ionic sensors. Compared with the initial and end stages (Insets of Fig. S10c), relative resistance changes of the sensors had no noticeable deterioration, indicating that the DHB-Fe2/CS1/PAA20 had a good reuse capability. Moreover, the response time is also an important parameter for ionic sensors. Our ionic sensor devices exhibited an immediate response to instantaneous stretching deformation (Fig. S11), with response time as low as 180 ms. Therefore, the DHB-Fe2/CS1/PAA20 sensor could detect over a wide range of tensile strains and demonstrated high sensitivity, fast response speed and significant cycling stability, making it an ideal candidate for stretchable ionic sensors.

As summarized in Table 2, the tensile strength and elongation at break of DHB-Fe/CS/PAA were comparable to those of ion conductive hydrogels in literature. The DHB-Fe/CS/PAA samples can withstand long-term stretching/releasing processes for 1000 cycles at a 50% strain, demonstrating its excellent mechanical properties and high fatigue resistance. The ionic conductivity of DHB-Fe2/CS1/PAA20 was comparable to most of ion conductive hydrogels in literature. Table 2 also showed the comparisons of sensing performances of our ionic sensor with ion conductive hydrogel-based sensors in literature. The GF value of the sensor was kept at 3.1 in a wide strain range of 300–500% and the sensitivity was comparable to other reported values. Considering the service environment of flexible devices, ionic sensors are damaged inevitably in practical applications. Therefore, self-healing ability is an important requirement of ionic sensors. To investigate the sensing ability after cutting and self-healing, the healed DHB-Fe2/CS1/PAA20 sensors were detected (Fig. 6d and e, S12). Notably, the resistance changes of the repaired sensor were similar to that of the original sensor, indicating that the resistance signals of the sensor could be completely recovered after healing.

Hydrogel samples were sandwiched between two pieces of VHB tapes to avoid the evaporation of water. The tape-encapsulated DHB-Fe2/CS1/PAA20 was directly assembled as an ionic sensor to monitor diverse human activities in real working environments because of its outstanding sensing performance over a broad range of strain. When the DHB-Fe2/CS1/PAA20 strain sensor was attached to the throat, it could monitor changes in electric signals when the volunteer swallowed (Fig. 6f). The output resistance signals exhibited remarkably characteristic patterns with good repeatability, reflecting the high sensitivity of the ionic sensors. The DHB-Fe2/CS1/PAA20 was further attached to a finger to detect bending motions at various angles (Fig. 6g). The bending behavior of the finger was distinctly monitored. Each finger motion, such as 30°, 60°, and 90° bending, could be distinguished with a large increase in resistance of the sensor at a higher bending angle, showing excellent reversibility along with fast response time. Similarly, large strains induced by bending of the opisthenar, wrist, elbow joint, and knee were also tracked from variations in relative resistance (Figs. 6h and S13). The transition points of all test curves were clear and obvious with remarkable reproducibility and stability.

To further demonstrate the flexibility and conductive performance of the anti-freezing DHB-Fe2/CS1/PAA20, the resistance changes under repeated stretching/releasing cycles with a 50% strain were studied at −25 °C (Fig. 6i). The DHB-Fe2/CS1/PAA20 sensor exhibited high sensitivity and good reproducibility, demonstrating its promising applications for detecting stretching and bending movements of human body at sub-zero temperatures. For example, real-time monitoring of the throat during swallowing could be recorded by the DHB-Fe2/CS1/PAA20 sensor without noise fluctuation or hysteresis (Fig. 6j). The DHB-Fe2/CS1/PAA20 sensor was tightly attached to the knuckle to detect finger flexion. The finger underwent rapid bending and releasing at −25 °C, and $\Delta R/R_0$ of the DHB-Fe2/CS1/PAA20 sensor synchronized perfectly with the finger bending (Fig. 6k), revealing its instantaneity and good stability. The DHB-Fe2/CS1/PAA20 sensor was used as a stretchable human motion detector through mounting on a hand in a −25 °C environment (Fig. 6l). The DHB-Fe2/CS1/PAA20 sensor collectively followed the strain of human skin, and deformation of skin was accurately recorded through the resistance changes. As a result, the anti-freezing DHB-Fe2/CS1/PAA20 sensor is promising for practical applications in wearable devices, which could monitor signals of bending and stretching in real-time and exhibit great potentials in a reliable artificial intelligence device in low-temperature environments. All these applications demonstrated the accurate sensing ability of the DHB-Fe2/CS1/PAA20 sensor for gentle motion (i.e., throat knot vibration) and large body movements (including finger bending, elbow bending, and knee bending), which might be useful in the diagnosis and physical therapy.

4. Conclusion

In summary, a DHB-Fe/CS/PAA with highly stretchable and compressive capabilities was fabricated through a hydrogen-bonded network densification strategy. In a typical procedure, the Fe/CS/PAA was prepared by a hydrogel network-constrained polymerization of anionic Fe-PAA network within cationic Fe-CS network. Benefiting from the formation of a densified hydrogen-bonded network between the Fe-PAA and Fe-CS chains activated by subsequent salt impregnation, the resultant DHB-Fe/CS/PAA exhibited high tensile strength of ~0.34 MPa, large stretchability of >1370%, and excellent fatigue resistance for 1000 cycles. The DHB-Fe/CS/PAA simultaneously possessed high mechanical

Table 2
Summary of mechanical properties, ionic conductivities and sensing performances of ion conductive hydrogel-based strain sensors.

Samples	Tensile cycles/ Strain	Tensile strength (MPa)	Tensile strain (%)	Ionic conductivity (S m^{-1})	Sensing cycles/ Strain	Gauge factor	Ref.
Laponite/PSBMA-co-HEMA	–	0.27	2000	0.24	–	1.8 (0–100%)	[53]
κ-CG/P(AAm-co-AAc)-Fe^{3+}	5/400%	2.7	1400	1.15	500/50%	0.78 (0%), 2.8 (500%)	[54]
PDA-clay-PSBMA	5/400%	0.09	900	0.02	–	1 (0–80%), 2.2 (300%)	[55]
P(AAm-HMA)	60/80%	0.62	2160	–	100/50%	0.74 (0–10%), 1.77 (10–60%), 2.57 (60–100%)	[56]
P(AAm-co-LMA)	5/500%	1.37	2058	1.79	300/50%	5.44 (0.25–2000%)	[57]
SA/NaCl/PAM	20/1000%	0.75	3120	0.01	500/50%	2 (200%), 2.7 (200–1800%)	[58]
CS/PAA/TA@CNC	10/350%	1.2	800	–	250/20%	3.0 (300%)	[44]
NaCl/SA/poly acrylic-acrylamide	–	0.27	1480	–	300/65%	0.65 (10%), 3.03 (1000%)	[59]
DHB-Fe2/CS1/PAA20	1000/50%	0.34	1375	0.24	500/100%	1.4 (0–100%), 2.2 (100–300%), 3.1 (300–500%)	This work

robustness, excellent fatigue resistance, heat-accelerated self-healability, and excellent sensitivity in ionic conductivity, which made it an ideal candidate as a wearable ionic strain sensor for detecting subtle human motions of finger bending and throat swallowing. The as-assembled DHB-Fe/CS/PAA ionic sensor exhibited high sensitivity (GF of 3.1), short response time (<180 ms), wide strain ranges (0.5–500%), low detection limit (<0.5%) and long-term cycles over 500 times of loading-unloading. Furthermore, the DHB-Fe/CS/PAA ionic sensor showed stable mechanical properties, stable ionic conductivity and sensing capabilities at sub-zero temperatures (−25 °C). Therefore, this work might provide an exploration for PECH with excellent fatigue resilience and self-healing for high-sensitivity and durable ionic sensing applications.

CRediT authorship contribution statement

Hui Song: Visualization, Investigation, Data curation, Writing – original draft. **Yinglun Sun:** Investigation, Writing – review & editing. **Jixin Zhu:** Investigation, Writing – review & editing. **Jingsan Xu:** Writing – review & editing. **Chao Zhang:** Conceptualization, Methodology, Supervision, Writing – review & editing. **Tianxi Liu:** Conceptualization, Supervision.

Declaration of competing interest

The authors declare that they have no known competing financial interests or personal relationships that could have appeared to influence the work reported in this paper.

Acknowledgments

This work was supported by the National Natural Science Foundation of China (21875033), the Fundamental Research Funds for the Central Universities (2232020G-02), the Shanghai Rising-Star Program (18QA1400200), and Ministry of Education of the People's Republic of China (6141A02033233).

Appendix A. Supplementary data

Supplementary data to this article can be found online at https://doi.org/10.1016/j.compositesb.2021.108901.

References

[1] Sun J-Y, Keplinger C, Whitesides GM, Suo Z. Ionic skin. Adv Mater 2014;26:7608–14.
[2] Park S, Parida K, Lee PS. Deformable and transparent ionic and electronic conductors for soft energy devices. Adv. Energy Mater. 2017;7:1701369.
[3] Qin Z, Sun X, Yu Q, Zhang H, Wu X, Yao M, Liu W, Yao F, Li J. Carbon nanotubes/hydrophobically associated hydrogels as ultrastretchable, highly sensitive, stable strain, and pressure sensors. ACS Appl Mater Interfaces 2020;12:4944–53.
[4] Kim D, Ahn S-K, Yoon J. Highly stretchable strain sensors comprising double network hydrogels fabricated by microfluidic devices. Adv Mater 2019;4:1800739.
[5] Lei Z, Wu P. A highly transparent and ultra-stretchable conductor with stable conductivity during large deformation. Nat Commun 2019;10:3429.
[6] Kim YM, Moon HC. Ionoskins: nonvolatile, highly transparent, ultrastretchable ionic sensory platforms for wearable electronics. Adv Funct Mater 2020;30:1907290.
[7] Cao Y, Morrissey TG, Acome E, Allec SI, Wong BM, Keplinger C, Wang C. A transparent, self-healing, highly stretchable ionic conductor. Adv Mater 2017;29:1605099.
[8] Yuan T, Cui X, Liu X, Qu X, Sun J. Highly tough, stretchable, self-healing, and recyclable hydrogels reinforced by in situ-formed polyelectrolyte complex nanoparticles. Macromolecules 2019;52:3141–9.
[9] Odent J, Wallin TJ, Pan W, Kruemplestaedter K, Shepherd RF, Giannelis EP. Highly elastic, transparent, and conductive 3d-printed ionic composite hydrogels. Adv Funct Mater 2017;27:1701807.
[10] Wang Z, Chen J, Wang L, Gao G, Zhou Y, Wang R, Xu T, Yin J, Fu J. Flexible and wearable strain sensors based on tough and self-adhesive ion conducting hydrogels. J Mater Chem B 2019;7:24–9.
[11] Song M, Yu H, Zhu J, Ouyang Z, Abdalkarim SYH, Tam KC, Li Y. Constructing stimuli-free self-healing, robust and ultrasensitive biocompatible hydrogel sensors with conductive cellulose nanocrystals. Chem Eng J 2020;398:125547.
[12] Du W, Zhang J, Zhao Z, Zhang X. Preparation of novel temperature-responsive double-network hydrogel reinforced with aramid nanofibers. Compos. Commun. 2020;22:100438.
[13] Hsiao L-Y, Jing L, Li K, Yang H, Li Y, Chen P-Y. Carbon nanotube-integrated conductive hydrogels as multifunctional robotic skin. Carbon 2020;161:784–93.
[14] Shi L, Jia K, Gao Y, Yang H, Ma Y, Lu S, Gao G, Bu H, Lu T, Ding S. Highly stretchable and transparent ionic conductor with novel hydrophobicity and extreme-temperature tolerance. Research 2020;2020:2505619.
[15] Jing X, Mi HY, Lin YJ, Enriquez E, Peng XF, Turng LS. Highly stretchable and biocompatible strain sensors based on mussel-inspired super-adhesive self-healing hydrogels for human motion monitoring. ACS Appl Mater Interfaces 2018;10:20897–909.
[16] Pan K, Peng S, Chu Y, Liang K, Wang CH, Wu S, Xu J. Highly sensitive, stretchable and durable strain sensors based on conductive double-network polymer hydrogels. J Polym Sci 2020;58:3069–81.
[17] Zhang B, Zhang X, Wan K, Zhu J, Xu J, Zhang C, Liu T. Dense hydrogen-bonding network boosts ionic conductive hydrogels with extremely high toughness, rapid self-recovery and autonomous adhesion for human-motion detection. Research 2021;2021:9761625.
[18] Zhao J, Chen Y, Yao Y, Tong Z-R, Li P-W, Yang Z-M, Jin S-H. Preparation of the polyelectrolyte complex hydrogel of biopolymers via a semi-dissolution acidification sol-gel transition method and its application in solid-state supercapacitors. J Power Sources 2018;378:603–9.
[19] Mao J, Zhao C, Li Y, Xiang D, Wang Z. Highly stretchable, self-healing, and strain-sensitive based on double-crosslinked nanocomposite hydrogel. Compos. Commun. 2020;17:22–7.
[20] Huang J, Peng S, Gu J, Chen G, Gao J, Zhang J, Hou L, Yang X, Jiang X, Guan L. Self-powered integrated system of a strain sensor and flexible all-solid-state supercapacitor by using a high performance ionic organohydrogel. Mater. Horiz. 2020;7:2085–96.
[21] Jian Y, Wu B, Le X, Liang Y, Zhang Y, Zhang D, Zhang L, Lu W, Zhang J, Chen T. Antifreezing and stretchable organohydrogels as soft actuators. Research 2019;2019:2384347.
[22] Zhang J, Zeng L, Qiao Z, Wang J, Jiang X, Zhang YS, Yang H. Functionalizing double-network hydrogels for applications in remote actuation and in low-temperature strain sensing. ACS Appl Mater Interfaces 2020;12:30247–58.
[23] Deng Y, Hussain I, Kang M, Li K, Yao F, Liu S, Fu G. Self-recoverable and mechanical-reinforced hydrogel based on hydrophobic interaction with self-healable and conductive properties. Chem Eng J 2018;353:900–10.
[24] Fan H, Wang J, Jin Z. Tough, swelling-resistant, self-healing, and adhesive dual-cross-linked hydrogels based on polymer–tannic acid multiple hydrogen bonds. Macromolecules 2018;51:1696–705.
[25] Zhang X-F, Ma X, Hou T, Guo K, Yin J, Wang Z, Shu L, He M, Yao J. Inorganic salts induce thermally reversible and anti-freezing cellulose hydrogels. Angew Chem Int Ed 2019;58:7366–70.
[26] Porath J, Sundberg L, Fornstedt N, Olsson I. Salting-out in amphiphilic gels as a new approach to hydrophobia adsorption. Nature 1973;245:465–6.
[27] Yang Y, Wang X, Yang F, Shen H, Wu D. A universal soaking strategy to convert composite hydrogels into extremely tough and rapidly recoverable double-network hydrogels. Adv Mater 2016;28:7178–84.
[28] Huang H, Han L, Li J, Fu X, Wang Y, Yang Z, Xu X, Pan L, Xu M. Super-stretchable, elastic and recoverable ionic conductive hydrogel for wireless wearable, stretchable sensor. J Mater Chem A 2020;8:10291–300.
[29] Ladet S, David L, Domard A. Multi-membrane hydrogels. Nature 2008;452:76–9.
[30] Kim ES, Song DB, Choi KH, Lee JH, Suh DH, Choi WJ. Robust and recoverable dual cross-linking networks in pressure-sensitive adhesives. J Polym Sci 2020;58:3358–69.
[31] Ding H, Li B, Liu Z, Liu G, Pu S, Feng Y, Jia D, Zhou Y. Nonswelling injectable chitosan hydrogel via uv crosslinking induced hydrophobic effect for minimally invasive tissue engineering. Carbohydr Polym 2021;252:117143.
[32] Chang Z, Chen Y, Tang S, Yang J, Chen Y, Chen S, Li P, Yang Z. Construction of chitosan/polyacrylate/graphene oxide composite physical hydrogel by semi-dissolution/acidification/sol-gel transition method and its simultaneous cationic and anionic dye adsorption properties. Carbohydr Polym 2020;229:115431.
[33] Wang A, Wang Y, Zhang B, Wan K, Zhu J, Xu J, Zhang C, Liu T. Hydrogen-bonded network enables semi-interpenetrating ionic conductive hydrogels with high stretchability and excellent fatigue resistance for capacitive/resistive bimodal sensors. Chem Eng J 2021;411:128506.
[34] Wang J, Tang F, Wang Y, Lu Q, Liu S, Li L. Self-healing and highly stretchable gelatin hydrogel for self-powered strain sensor. ACS Appl Mater Interfaces 2020;12:1558–66.
[35] Li L, Zhang Y, Lu H, Wang Y, Xu J, Zhu J, Zhang C, Liu T. Cryopolymerization enables anisotropic polyaniline hybrid hydrogels with superelasticity and highly deformation-tolerant electrochemical energy storage. Nat Commun 2020;11:62.
[36] Guo H, Feng Q, Xu K, Xu J, Zhu J, Zhang C, Liu T. Self-templated conversion of metallogel into heterostructured tmp@carbon quasiaerogels boosting bifunctional electrocatalysis. Adv Funct Mater 2019;29:1903660.
[37] Darabi MA, Khosrozadeh A, Mbeleck R, Liu Y, Chang Q, Jiang J, Cai J, Wang Q, Luo G, Xing M. Skin-inspired multifunctional autonomic-intrinsic conductive self-healing hydrogels with pressure sensitivity, stretchability, and 3d printability. Adv Mater 2017;29:1700533.
[38] Zhao L, Jiang B, Huang Y. Self-healable polysiloxane/graphene nanocomposite and its application in pressure sensor. J Mater Sci 2019;54:5472–83.

[39] Zhou Y, Wan C, Yang Y, Yang H, Wang S, Dai Z, Ji K, Jiang H, Chen X, Long Y. Highly stretchable, elastic, and ionic conductive hydrogel for artificial soft electronics. Adv Funct Mater 2019;29:1806220.
[40] Huang Y, Zhong M, Huang Y, Zhu M, Pei Z, Wang Z, Xue Q, Xie X, Zhi C. A self-healable and highly stretchable supercapacitor based on a dual crosslinked polyelectrolyte. Nat Commun 2015;6:10310.
[41] Wang X-H, Song F, Qian D, He Y-D, Nie W-C, Wang X-L, Wang Y-Z. Strong and tough fully physically crosslinked double network hydrogels with tunable mechanics and high self-healing performance. Chem Eng J 2018;349:588–94.
[42] Yang J, Chen Y, Zhao L, Feng Z, Peng K, Wei A, Wang Y, Tong Z, Cheng B. Preparation of a chitosan/carboxymethyl chitosan/agnps polyelectrolyte composite physical hydrogel with self-healing ability, antibacterial properties, and good biosafety simultaneously, and its application as a wound dressing. Compos B Eng 2020;197:108139.
[43] Tang S, Yang J, Lin L, Peng K, Chen Y, Jin S, Yao W. Construction of physically crosslinked chitosan/sodium alginate/calcium ion double-network hydrogel and its application to heavy metal ions removal. Chem Eng J 2020;393:124728.
[44] Cui C, Shao C, Meng L, Yang J. High-strength, self-adhesive, and strain-sensitive chitosan/poly(acrylic acid) double-network nanocomposite hydrogels fabricated by salt-soaking strategy for flexible sensors. ACS Appl Mater Interfaces 2019;11:39228–37.
[45] Zhang Z, Gao Z, Wang Y, Guo L, Yin C, Zhang X, Hao J, Zhang G, Chen L. Eco-friendly, self-healing hydrogels for adhesive and elastic strain sensors, circuit repairing, and flexible electronic devices. Macromolecules 2019;52:2531–41.
[46] Liu H, Wang X, Cao Y, Yang Y, Yang Y, Gao Y, Ma Z, Wang J, Wang W, Wu D. Freezing-tolerant, highly sensitive strain and pressure sensors assembled from ionic conductive hydrogels with dynamic cross-links. ACS Appl Mater Interfaces 2020;12:25334–44.
[47] Morelle XP, Illeperuma WR, Tian K, Bai R, Suo Z, Vlassak JJ. Highly stretchable and tough hydrogels below water freezing temperature. Adv Mater 2018;30:1801541.
[48] Wu J, Wu Z, Wei Y, Ding H, Huang W, Gui X, Shi W, Shen Y, Tao K, Xie X. Ultrasensitive and stretchable temperature sensors based on thermally stable and self-healing organohydrogels. ACS Appl Mater Interfaces 2020;12:19069–79.
[49] Li Ra, Chen G, Fan T, Zhang K, He M. Transparent conductive elastomers with excellent autonomous self-healing capability in harsh organic solvent environments. J Mater Chem A 2020;8:5056–61.
[50] Wang Y, Tebyetekerwa M, Liu Y, Wang M, Zhu J, Xu J, Zhang C, Liu T. Extremely stretchable and healable ionic conductive hydrogels fabricated by surface competitive coordination for human-motion detection. Chem Eng J 2020. https://doi.org/10.1016/j.cej.2020.127637.
[51] Pourjavadi A, Tavakolizadeh M, Hosseini SH, Rabiee N, Bagherzadeh M. Highly stretchable, self-adhesive, and self-healable double network hydrogel based on alginate/polyacrylamide with tunable mechanical properties. J Polym Sci 2020;58:2062–73.
[52] Liu Z, Wan K, Zhu T, Zhu J, Xu J, Zhang C, Liu T. Superelastic, fatigue-resistant, and flame-retardant spongy conductor for human motion detection against a harsh high-temperature condition. ACS Appl Mater Interfaces 2021;13:7580–91.
[53] Wang L, Gao G, Zhou Y, Xu T, Chen J, Wang R, Zhang R, Fu J. Tough, adhesive, self-healable, and transparent ionically conductive zwitterionic nanocomposite hydrogels as skin strain sensors. ACS Appl Mater Interfaces 2019;11:3506–15.
[54] Zhou L, Wang Z, Wu C, Cong Y, Zhang R, Fu J. Highly sensitive pressure and strain sensors based on stretchable and recoverable ion-conductive physically cross-linked double-network hydrogels. ACS Appl Mater Interfaces 2020;12:51969–77.
[55] Pei X, Zhang H, Zhou Y, Zhou L, Fu J. Stretchable, self-healing and tissue-adhesive zwitterionic hydrogels as strain sensors for wireless monitoring of organ motions. Mater. Horiz. 2020;7:1872–82.
[56] Zhang Q, Liu X, Ren X, Jia F, Duan L, Gao G. Nucleotide-regulated tough and rapidly self-recoverable hydrogels for highly sensitive and durable pressure and strain sensors. Chem Mater 2019;31:5881–9.
[57] Xia S, Zhang Q, Song S, Duan L, Gao G. Bioinspired dynamic cross-linking hydrogel sensors with skin-like strain and pressure sensing behaviors. Chem Mater 2019;31:9522–31.
[58] Zhang X, Sheng N, Wang L, Tan Y, Liu C, Xia Y, Nie Z, Sui K. Supramolecular nanofibrillar hydrogels as highly stretchable, elastic and sensitive ionic sensors. Mater. Horiz. 2019;6:326–33.
[59] Huang H, Han L, Fu X, Wang Y, Yang Z, Pan L, Xu M. Multiple stimuli responsive and identifiable zwitterionic ionic conductive hydrogel for bionic electronic skin. Adv. Electron. Mater. 2020;6:2000239.